AUT Journal of Electrical Engineering

AUT J. Elec. Eng., 51(2) (2019) 161-170
DOI: 10.22060/eej.2019.15766.5267

A Novel Sampling Approach in GNSS-RO Receivers with Open Loop Tracking Method

L. Mohammadi[1,*], Sh. Amiri[2]

[1] Assistant Professor, Iran Telecommunication Research Center(ITRC), Tehran, Iran.
[2]Associate Professor, Iranian Research Organization for Science and Technology(IROST), Tehran, Iran.

ABSTRACT: Propagation of radio occultation (RO) signals through the lower troposphere results in high phase acceleration and low signal to noise ratio signal. The excess Doppler estimation accuracy in lower troposphere is very important in receiving RO signals which can be estimated by sliding window spectral analysis. To do this, various frequency estimation methods such as MUSIC and ESPRIT can be adopted. Due to the cost and bandwidth constraints, reducing the sampling rate at GNSS receivers of LEO satellite is necessary which causes aliasing. A method of resolving frequency ambiguities is the simultaneous sampling of signal by multiple sample frequencies (MSF). Accordingly, we study the capacity of MSF method to improve the spectral efficiency and use accurate frequency estimation schemes to enhance the excess Doppler estimation accuracy of RO signal in post-processing. Via simulation results, the accuracy of excess Doppler estimation in post-processing based on both single sample frequency (SSF) and MSF methods for different frequency estimation methods are compared. Simulation results reveal that the MSF method has better performance than that of the SSF method. Besides, it is shown that Jacobsen and Jacobsen with Bias methods almost have the same performance and their estimation error is less than that of other methods. By exploiting the proposed scheme, the frequency estimation error is significantly decreased and it is negligible compared to the traditional methods. Moreover, by using this scheme, we have 41.6% bandwidth saving.

Review History:
Received: 2019-02-03
Revised: 2019-07-31
Accepted: 2019-09-04
Available Online: 2019-12-01

Keywords:
Radio occultation
Frequency estimation
Multi rate sampling frequency
Open loop tracking

1- Introduction

1-1- Motivation

Excess Doppler is the main parameter in the RO signal processing which can be inverted to atmospheric parameters, such as pressure, temperature or water vapor profiles. The phase difference between a local signal replicas generated from a reference Doppler model in open-loop (OL) tracking and received signals at GNSS receiver is defined as the excess phase which is calculated by differentiating the excess phase observations. Propagation of RO signals through the lower troposphere results in high excess Doppler and low signal to noise ratio (SNR) signal. In tracking of RO signals, another important parameter is phase acceleration which is the derivative of the signal's phase and represents the rate at which the signal's phase changes. Note that the value of this parameter in the lower troposphere is more than 2 kHz/s. If the phase acceleration is more than 300 Hz/s, the phase-locked loop (PLL) in conventional GNSS survey receivers loses phase lock. To tackle this issue, in low SNR and high dynamic Doppler, OL tracking is introduced [1-5]. This method relies on a priori models of Doppler shift. Since the bandwidth of the signal may vary with lower tropospheric conditions, the down converted signal should be sampled based on the suitable frequency sampling rate and then sent to ground-based processing unit. In fact, the higher sampling rate with accurate model of Doppler, enables monitoring of lower troposphere and improves the accuracy of weather prediction [3, 6]. However, high sampling rate would demand huge amounts of bandwidth and require additional ground-based processing and cost. Therefore, due to the cost constraints and limitation on the amount of information sent to the ground, reducing the sampling rate is very appealing. For this reason, we try to enhance the accuracy of the Doppler predicted models while reducing the sampling rate [3, 6].

In the new RO receivers such as Integrated GPS Occultation Receiver (IGOR) and RO Sounder for Atmospheric studies (ROSA), the sampling rate is chosen to be 100 Hz. Also, in the GNSS occultation reflectometry and scatterometry (GORS) RO receiver, the sampling rate is set to 200 Hz [7]. Since we cannot increase the accuracy of frequency estimation in the specific climatic conditions, to achieve more atmospheric parameters, a higher sampling rate is necessary. In other words, by increasing the sampling rate, more atmosphere information can be obtained at the expense of larger bandwidth. To determine neutral atmospheric parameters, estimation of excess Doppler is necessary in post–processing stage. The accuracy of excess Doppler is very important in achieving of precise atmospheric profiles. In this regard, we need to use accurate frequency estimation

*Corresponding author's email: mohamady@itrc.ac.ir

methods. The excess Doppler can be estimated by sliding window spectral analysis. In this method, the position of the main spectral peak in subsequent spectra is derived. To do this, there are many methods such as multiple signal classification (MUSIC), Estimation of Signal Parameters via Rotational Invariance Techniques (ESPRIT), etc. If a RO signal is sampled at a sampling rate which is smaller than the excess Doppler, ambiguities appear in the sampled data. To cope with this ambiguity in a bandwidth limited situation, we adopt a powerful sampling method called multiple sample frequencies (MSF) which is able to remove ambiguities by increasing the Doppler frequency estimation range.

1-2- Related Works

In [6, 8, 9], the authors obtained estimation of Doppler shift frequency based on the variations of amplitude and phase of the received signal. Propagation of RO signals through the moist troposphere results in strong fluctuation of the phase and amplitude [8]. Analysis of Doppler frequency results in ~ ± 50 kHz and ~ ± 2 kHz geometric and atmospheric Doppler shift, respectively [6], [8]. The instability of the PLL tracking in the troposphere motivated the authors in [6, 10, 11] to consider the OL tracking.

The principles of the OL tracking of RO signals outlined in [6] include estimates of the necessary filter bandwidth and sampling rate. In real time, a RO signal must be subject to down-conversion in receiver, by use of the pre-calculated phase model, without a feedback from the received signal. Then, the down-converted RO signal is low-pass filtered, sampled and transmitted to the ground station for post–processing.

In previous related works, the Single Sample Frequency (SSF) sampling method is used for sampling the RO signal. However, in some cases, the excess Doppler exceeds the sampling rate, resulting in frequency ambiguities in post–processing and subsequently error in the extracted atmosphere profile. To cope with this in post–processing, radio holography (RH) methods are suggested to process RO data in atmospheric multipath zones and to improve retrieval accuracy in the moist lower troposphere [12]: back propagation (BP) [13, 14], sliding spectral (SS) [6], canonical transform (CT) [15, 16], full spectrum inversion (FSI) [17, 18], CT2 [19] and phase matching (PM) [20]. The SS method can be accounted for the whole spectrum of the signals in the small window. Different frequency estimation methods such as MUSIC is used to test the SS method by processing 4 GPS/MET occultations [21]. The bias induced by the noise in RH is investigated in [22]. However, false spectral maxima can cause retrieval errors in the SS method. Therefore, accuracy of frequency estimation is very important in the SS and other methods. However, in some cases, the excess Doppler estimation by using this method does not have enough precision which results in random and systematic error (bias) in the extracted phase and in the retrieved refractivity. The sparse sampling method is another one to circumvent Nyquist and perfectly sample and reconstruct signals [23]. However, as mentioned in [23], the sparse sampling method leads to a loss of performance (about 5 dB SNR).

Frequency estimation methods can be grouped into two main categories: parametric (high-resolution) methods and non-parametric (periodogram-based) methods. Nonparametric frequency estimation methods are based on the Fourier transform of the data sequence or its autocorrelation function. The FFT makes it convenient to calculate the periodogram spectral estimate or any of its variations [24]. Classical non-parametric spectral estimators are still the most robust for low SNR region [25]. In addition, these methods are applicable to all signal classes and the estimated power spectral density (PSD) is directly proportional to power. The main disadvantage of these methods is their low resolution limited by windowing effects. MUSIC and ESPRIT are high-resolution methods which are intended for estimating spectral lines (frequencies) [26, 27].

Various fine-frequency estimators have been proposed in the literature [28, 29, 30,31]. The authors in [28] use the complex Fourier coefficients in order to interpolate the true signal frequency between the maximum and the second highest bin. However, Quinn's algorithm has been shown to have a frequency dependent performance [32]. The Parabolic method uses three DFT magnitude samples [35], [36] to estimate location of peak. In the Jacobsen Method, in order to increase the accuracy of peak value location estimation, the complex DFT values rather than the magnitudes are used [34]. Quinn method [28], Macleod method [29], Jacobsen with Bias method [37] and ESPRIT method [38], [39] are proposed in previous literature. In our previous paper [33], we investigated the aforementioned frequency estimation methods and compared performance of them in the SSF scheme. In this paper, we investigated the performance of using these methods in the MSF scheme. To the best of our knowledge, there is no related works on the Doppler frequency estimation via the MSF method.

1-3- Our Contributions

In this paper, we study the potential benefits of MSF method in the estimation of Doppler frequency, with the goal of minimizing frequency estimation error in bandwidth limited situation. Besides, we compare the MSF method with the SSF method in LEO receiver from computational complexity and performance and we also evaluate the performance and computational complexity of different frequency estimation methods. To the best of our knowledge, no work has investigated the SSF and MSF methods to improve the estimates of the Doppler frequency in post–processing.

The paper is organized as follows. In Section 2, we investigate RO signal processing by using OL tracking. Then, in Section 3, we investigate the MSF method. Simulation results are presented in Section 4. The computational complexity of the proposed methods is studied in Section 5, and conclusions are provided in Section 6.

2- RO Signal Processing by Using OL Tracking

In OL tracking, the signal is down-converted via a numerically controlled oscillator (NCO), which produces

Fig 1. Block diagram of the RO data processing.

a frequency given by an on-board Doppler model pre-calculated in GNSS receiver without a feedback from the received signal. Next, in order to remove the noise from data, i.e., on amplitude and phase of signal, a zero-phase low-pass filter is adopted.

The baseband signal is then sampled at a predetermined rate. After the down-converted RO signal is passed through a low-pass filter, the sampled in-phase (I) and quadrature (Q) components, are transmitted to the ground (along with the Doppler model) for post–processing.

In Fig. 1, block diagram of the RO data processing for OL tracking is shown. As can be seen, various steps of processing is needed to estimate atmospheric parameters. The main focus of this paper is related to the Steps 2 and 4. We study new sampling frequency and estimation methods to reach the following aims:

I. Decreasing the required number of samples that should be transmitted from the LEO to the ground post–processing center.

II. Extending the Doppler frequency estimation range

III. Increasing the accuracy of frequency Doppler estimation in the new method of sampling.

To achieve the goals of I and II, we investigate the MSF method at which sampling is done by two different low sampling frequencies while in the traditional method, SSF is adopted at which the signal is only sampled with a higher frequency. For example, in SSF, the signal is sampled at 100 Hz while in MSF, the signal is simultaneously sampled at 30 and 40 Hz. The number of samples is reduced from 4000 samples that is 100 samples per second for 40 sec to 2800 sample per second by adopting MSF instead of SSF. Indeed, in MSF, it is equivalent to do sampling at 120 Hz while we only use the signal bandwidth of 70 Hz for sampling. In fact, the sampling rate of SSF is equal to the signal bandwidth. Consequently, by using MSF, we can save the satellite resources like power budget and bandwidth by decreasing the required number of samples that should be transmitted from the LEO to the ground post–processing center.

Furthermore, in some conditions of low troposphere, where the value of excess Doppler shift is more than 70 Hz, we cannot accurately extract the atmosphere parameters with 70 Hz SSF sampling. On the contrary, by using the MSF method, we can estimate the excess Doppler by 120 Hz via sampling rates of 30 Hz and 40 Hz simultaneously. Therefore, when the signal bandwidth is the same for both the SSF and MSF methods, we can achieve more valuable information about atmosphere parameters in MSF compared to the SSF. Accordingly, by using MSF, we can extend the Doppler frequency estimation range.

In the ground post–processing, extraction of excess phase for obtaining atmosphere parameters is very crucial. To do this, we need to use precise frequency estimation methods. Note that at the low troposphere conditions, the value of phase acceleration is high and the value of SNR is very low. These conditions make the excess Doppler estimation very difficult and challenging. To overcome this condition, an appropriate frequency estimation method should be adopted. In this regard, we study six frequency estimation methods, named ESPRIT, Jacobsen, Jacobsen with bias, Macleod, Quinn, and parabolic which have not been investigated in the existing

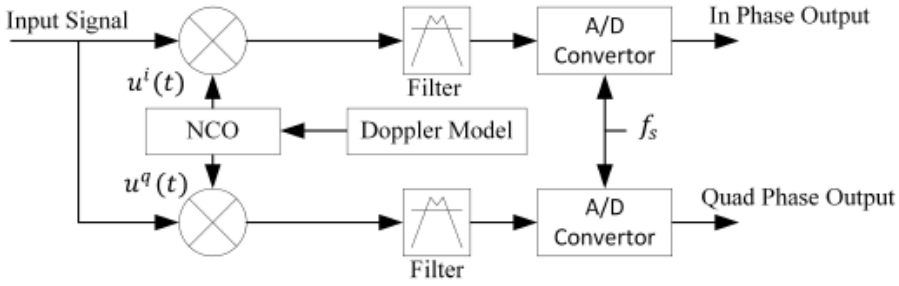

Fig 2. A schematic diagram of a LEO receiver with one Sampling frequency.

works. Based on our analysis in this situation, ESPRIT and Jacobsen with bias have result in higher accuracy than that of other methods. Accordingly, we can reach the goal of III by selecting accurate frequency estimation methods.

We use global position system (GPS) satellite signal on *L*1 (1575.42 MHz) frequency. When GPS-RO signals are used for monitoring the lower troposphere, the ionospheric effect has to be removed. Thus, GPS *L*1 signal is enough for the processing. In this paper, all calculations are provided for GPS *L*1 frequency; thus, only processing of *L*1 signal will be discussed. Based on Doppler shift model, the received signal is compared with NCO carriers phase-shifted with 90 degrees relative to each other and *I* and *Q* components are determined. The Doppler frequency of the received GPS signal relies on atmospheric condition and relative velocity of satellites.

The signal must be down-converted in the receiver with the use of the frequency model, $f_{mod} = fc + f_{dop}$, based on predicted GPS and LEO orbits and refractivity climatology. To minimize noise aliasing, it must be at first low-pass filtered, then are sampled and transmitted to the ground [6], [8]. The sampling rate generally has to be equal to the bandwidth of the signal. However, since the spread part of the spectrum occupies only part of the full spectral band, the sampling rate may be lower. When the sampling rate is greater or equal to the full spectral bandwidth of the signal, the spectrum is reproduced without aliasing and the signal may be completely recovered from its complex samples. Lower sampling rates may result in aliasing of harmonics in the signal spectrum. However, if the sampling rate is not less than the spread part of the spectrum (where most of the signal power is concentrated), then aliasing will not result in overlapping of harmonics [6], [8]. Therefore, by additional down-conversion, the signal can be recovered from its samples with minimal errors, which eliminates or reduces the aliasing. When sampling rate is smaller than the speared part of the spectrum, the signal cannot be recovered without being corrupted [6], [8]. In Fig. 2, OL tracking receiver schematic is shown, in which the receiver tracks the signal $u(t)$ by correlating $u(t)$ with replica signals $u^i(t)$ and $u^q(t)$

$$u^i(t) = \cos\left(\phi_{NCO}(t)\right), \tag{1}$$

$$u^q(t) = \sin\left(\phi_{NCO}(t)\right), \tag{2}$$

where phase ϕ_{NCO} is generated in the oscillator based on the Doppler model. NCO is driven by a-priori Doppler frequency model [6], [8], [10]. Then, the down-converted signal is passed through the low pass filter. The received signal is sampled and sent to the post– processing at the ground station. In order to remove navigation data modulation (NDM), the sampled signal must be down-converted to shift its mean frequency as close to zero as possible.

The purpose of this down-conversion is to remove NDM and connect the phase between samples. NDM can be removed using the internal or external methods [10]. Then, in post–processing, the received signal is down-converted by the use of a more accurate phase model. Signal phase and amplitude can be obtained as follows [10]

$$A = \left[\mathcal{R}\left\{u(t)\right\}^2 + \mathcal{I}\left\{u(t)\right\}^2\right]^{1/2}, \tag{3}$$

$$\phi = \arctan 2\left[\mathcal{I}\left\{u(t)\right\} / \mathcal{R}\left\{u(t)\right\}\right], \tag{4}$$

where $\mathcal{R}\{u\}$ and $\mathcal{I}\{u\}$ return the real and imaginary parts of u, respectively. High-resolution signal parameter estimation is necessary in many signal processing applications. Such applications include Doppler frequency estimation at post–processing stage in the RO occultation system. Retrieval of atmospheric parameters from RO data often encounters difficulties in the moist lower troposphere. Under conditions of atmospheric multipath propagation, calculation of bending angle from Doppler frequency shift is usually not applicable. The SS method uses spectral analysis of the received signals in small sliding apertures. As a function of the impact parameter, the bending angle is computed from the frequency of each spectral maximum and its corresponding position at the aperture center. Sorting out the doubtful maxima can improve accuracy of the SS method, especially in the lower troposphere [33]. Therefore, high resolution excess Doppler estimation is important at post–processing stage of the RO system and especially in the SS method.

3- Multiple Sample Frequencies Sampling Method

In the related literature, most of the works used the SSF

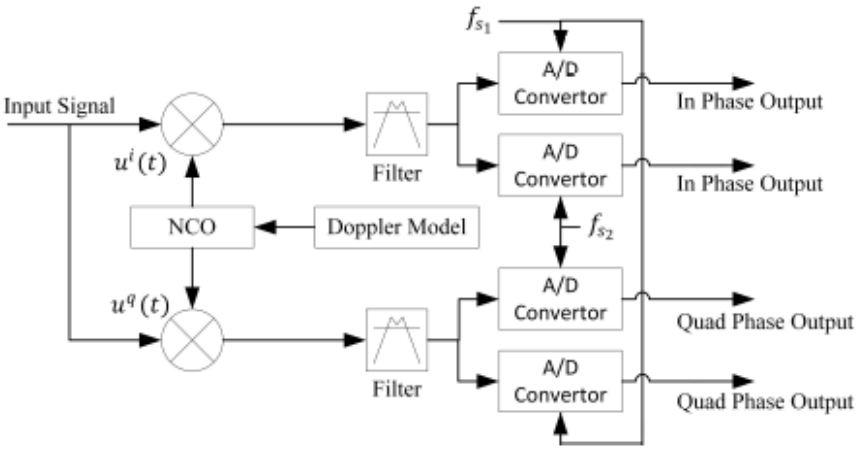

Fig 3. A schematic diagram of a LEO receiver with two Sampling frequencies.

sampling method in the LEO's receiver. In this receiver, the signal must be sampled in a rate that is greater than the biggest frequency component in the complex signal [6, 11]. However, due to the cost constraints and limitation on the amount of information sent to the post–processing center, reducing the sampling rate is required. For this reason, we try to enhance the accuracy of the Doppler predicted models in the satellite which makes the GNSS-RO receivers very complicated. Recently, receivers achieve higher resolution at higher sampling rates. In some cases, in RO, the excess Doppler exceeds the available bandwidth which results in frequency ambiguities. To overcome this difficulty and resolve this frequency ambiguities, the MSF method is used to sample an analogy signal with different rate simultaneously.

To reduce the system cost and avoid frequency ambiguities, in this section, we consider the MSF sampling method with sampling at multiple rate below the Nyquist frequency [40-43] By multiple frequencies sampling method, we can reduce the required bandwidth, which results in reducing system cost. In many receivers, the information bandwidth of signal to be processed is much narrower than the instantaneous bandwidth of the receiver, allowing the sampling signal at a rate below the Nyquist criteria. Thereby, this method makes very efficient use of A/D convertor and materially reduces the costs [41]. In this method, the signal is first sampled by the MSF method. However, sub-Nyquist rate sampling has the undesirable effect of folding the frequency components of the sampled signal into the fundamental range between $\pm fs/2$ and, consequently, causing ambiguities [41]. Although there is no way to resolve these ambiguities by using one set of data, they can be tackled by sampling the signal more than once. On the other hand, usage of sub-Nyquist rate sampling reduces the bandwidth of the digital processing components. The maximum achievable unambiguous bandwidth, when complex sampling is used, is equal to the product of the sample frequencies divided by their greatest common multiplier (GCM). For a given set of sample frequencies, the maximum achievable unambiguous bandwidth using real sampling is one half the achievable bandwidth using complex sampling. The schematic of digital receiver with two sampling frequencies is illustrated in Fig. 3. Comparing Fig. 3 with Fig. 2,, it can be seen that the signal is fed to each pair of circuits, one being 90 degrees out of phase with the order to provide an *I* input in one of the circuit and a *Q* input to the other circuit. Each of the circuits includes a low pass filter, and the output of each filter is passed to a pair of A/D convertors in each circuit, one of convertors being sampled at a sampling frequency $fs1$ and the other convertor being sampled at a sampling frequency $fs2$.

The outputs of the convertors are then processed. When the input signal is near an aliasing border, this method uses MSF to directly resolve the frequency ambiguity. By using two sampling frequencies, the maximum unambiguous frequency is given by

$$f_{unambig(max)} = \frac{f_{s1} f_{s2}}{GCM}, \tag{5}$$

where GCM is the greatest common multiplier between the two sample frequencies. This technique can be extended to *D* sample frequencies, thus the achievable maximum unambiguous frequency becomes a function of *D* sample frequencies which is given by

$$f_{unambig(max)} = \frac{\prod_{i=1}^{D} f_{si}}{GCM}, \tag{6}$$

Note that although higher unambiguous frequency can be achieved by MSF, this can increase the computational complexity, signal processing time, and system cost. The baseband frequency measurement, f_{meas} can be achieved directly or by use of a FFT or other digital signal processing techniques to provide signal processing gain. An integer, *M* or *N*, is returned from the lookup table which is used in one of the two following formulas to yield the unambiguous input frequency.

$$f_{unambig} = Mf_{s1} + f_{meas(f_{s1})} \tag{7}$$

$$f_{unambig} = Nf_{s2} + f_{meas(f_{s2})} \quad (8)$$

The construction of the lookup table is shown in Fig. 4. As shown, the ambiguity map represents the mapping of the input signal bandwidth into the sample frequency bandwidth of each sample frequency. The ambiguity map is constructed with the sample frequency bandwidth of the first sample frequency along the X axis and the sample frequency bandwidth of the second sample frequency along the Y axis. For complex sampling, the sample frequency bandwidth extends from zero to the sampling frequency. Beginning at origin, all input signal frequencies to the maximum unambiguous frequency are mapped into the spaces defined by the two axes. As the input signal frequency increases from zero, a diagonal line is traced which projects at 45 degrees upward and to the right. This first line represents an unaliased frequency measurement at both sample frequencies and the frequency measured at each sample frequency would be the same and equal to the frequency of the input signal.

This first line is labelled (0, 0) to denote that the frequency measurement in both sample rates is unaliased. When the input signal frequency is equal to one of the sample rates, the projection reaches a boundary indicating that the frequency measurement along that axis is now aliased. As an example of the utility of the map, an input signal at 110 Hz is mapped on each axis in Fig. 4, [41]. A 110 Hz signal sampled at 40 Hz and 30 Hz will indicate aliased frequencies of 30 Hz and 20 Hz, respectively. Sampling frequencies of $fs1$ = 40 Hz and $fs2$ = 30 Hz are considered. From (5), the maximum unambiguity frequency for this case is $f_{unambig}(max)$ = 120 Hz. Each projection in the map is shown by two integer values M and N. The lookup table needs only one of these integer values as reference. A unique position on the map is identified by the intersection of a vertical projection at $f_{meas}(f_{s1})$ (vertical dashed line at $f_{meas}(f_{s1})$ = 30 Hz) and a horizontal projection at $f_{meas}(f_{s2})$ (vertical dashed line at $f_{meas}(f_{s2})$ = 40 Hz). The ambiguity projection closet to this intersection gives the required value of M and N to take care of the frequency ambiguity.

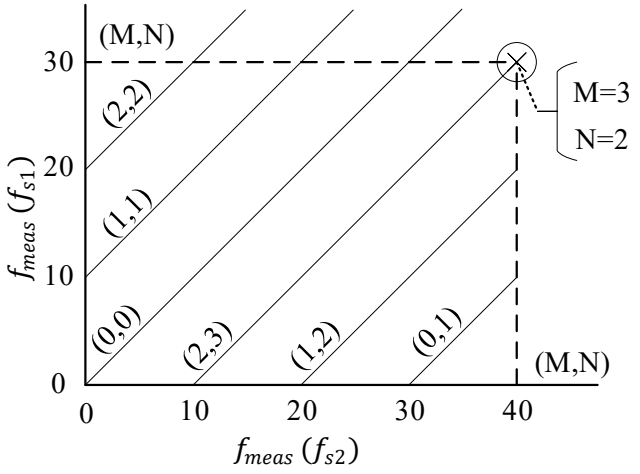

Fig 4 A typical signal ambiguity map (Lookup Table).

Table 1. Simulation setting.

Parameter name	Value
Phase accelaration	-2000 Hz/s to 2000 Hz/s
SNR	-10 dB to 20 dB
LEO altitude	400 km to 1500 km
Excess Doppler	-60 Hz to 60 Hz
Occultation time duration	T=40 sec
Length of the window	N=4 samples

4- Simulation Results

In this section, we perform the Monte Carlo based-simulations to evaluate the performance of both SSF and MSF with various frequency estimation methods. All the results are averaged on S independent runs. In other words, RMSE is estimated using 1000 Monte Carlo runs. Moreover, we present some simulation results to compare the performance of the six frequency estimation methods for both the SSF and MSF sampling schemes. We model the GNSS receiver's input as the sum of simulated signal and white Gaussian noise. The simulated signal is a multi-tone signal with time varying phase acceleration. The initial phase is 0. Simulation setting is shown in Table 1.

4-1 Effect of SNR on the Estimation Error

Here, we illustrate the effect of different values of SNR on the frequency estimation error for both the SSF and MSF sampling schemes. Fig. 5(a) shows RMSE versus SNR of the frequency estimation methods for the SSF sampling scheme. As can be seen, by increasing SNR, the frequency estimation error for all frequency estimation methods are decreased. ESPRIT and Jacobsen with bias methods have better performance than other methods. As shown in Fig. 5(a), the ESPRIT method mainly has the same accuracy as Jacobsen with bias method. In low SNR, both the Parabolic and Quinn methods are not robust to noise. Thus, these methods have higher frequency estimation error than that of the other methods. Fig. 5(b) shows RMSE versus SNR for the six frequency estimation methods in the MSF sampling scheme. As can be seen and as expected, the frequency estimation error gets smaller as SNR increases for all methods. The poorest performance belongs to the parabolic estimator. Moreover, the estimation by ESPRIT, and Jacobsen with Bias almost have the same error value in the same SNR and they have better performance than the other methods. Fig. 6(a) illustrates the benefit of the MSF sampling method in the receiver by comparing the frequency estimation error obtained by both the SSF and MSF sampling schemes. At SNR between 20 dB and -5 dB, the MSF scheme performance is better than that of the uniform scheme. Obviously, as also seen from Fig. 6(a), when we try to increase the value of SNR, RMSE of all frequency estimation algorithms is decreased. We also compare the SSF and MSF sampling schemes for various simulation parameters.

Excess Doppler is assumed to be between -45 Hz to 45

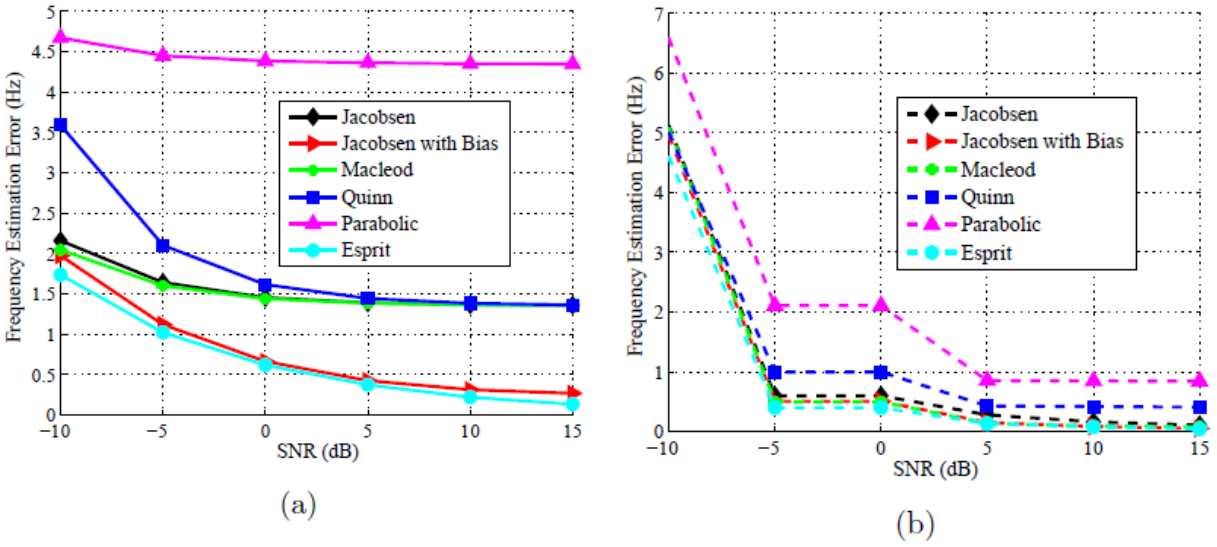

Fig 5. (a) Frequency estimation error versus SNR for different estimation algorithms of the SSF sampling scheme. System parameters: phase acceleration is between -2000 Hz/s and 2000 Hz/s and sampling frequency rate is 100 Hz. (b) Frequency estimation error versus SNR for different estimation algorithm of the MSF sampling scheme. System parameters: phase acceleration is between -2000 Hz/s and 2000 Hz/s and sampling frequencies are 30 Hz and 40 Hz.

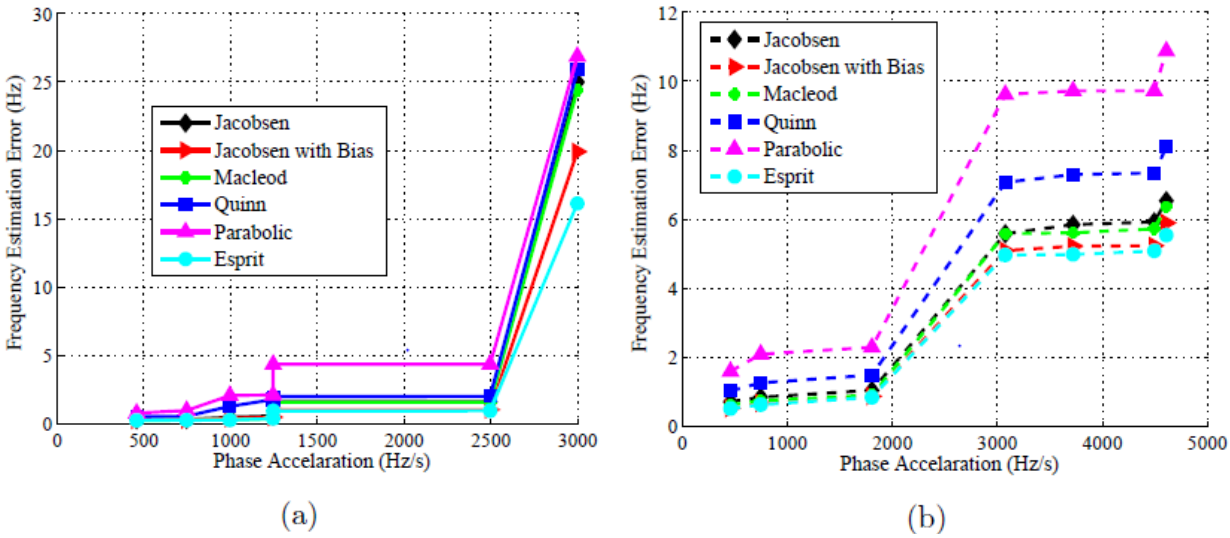

Fig 6. (a) Comparing the frequency estimation error for different estimation algorithms of both SSF and MSF sampling schemes. System parameters: phase acceleration is between −2000 Hz/s and 2000 Hz/s and sampling frequencies are 100 Hz and (30 Hz and 40 Hz) for both SSF and MSF sampling schemes, respectively. (b) Comparing the frequency estimation error for different estimation algorithms of both SSF and MSF sampling schemes. System parameters: phase acceleration is between -2000 Hz/s and 2000 Hz/s and sampling frequencies are 75 Hz and (30 Hz and 40 Hz) for both SSF and MSF sampling schemes, respectively.

Hz. As shown in Fig. 6(b), for new simulation parameters (Sampling rates are 75 Hz and 30 Hz and 40 Hz for both the SSF and MSF sampling schemes, respectively.), the MSF sampling method has better performance than the SSF scheme at the whole SNR range. Because in the MSF method, when the signal is sampled at 30 Hz and 40 Hz, it is as if we do sampling at 120 Hz (we can detect excess Doppler at 120 Hz without generating any ambiguity) while we only use the signal bandwidth of 70 Hz. This is while in the SSF method, when signal is sampled at 70 Hz, we are only able to detect the excess Doppler at 70 Hz. Accordingly, by using MSF, we can extend the Doppler frequency estimation range and reduce the frequency estimation error.

4-2- Effect of Phase Acceleration on the Frequency Estimation Error

Here, we illustrate the effect of phase acceleration on the frequency estimation error for both the SSF and MSF sampling schemes. Fig. 7(a) shows RMSE versus phase acceleration for the six frequency estimation methods based on the SSF

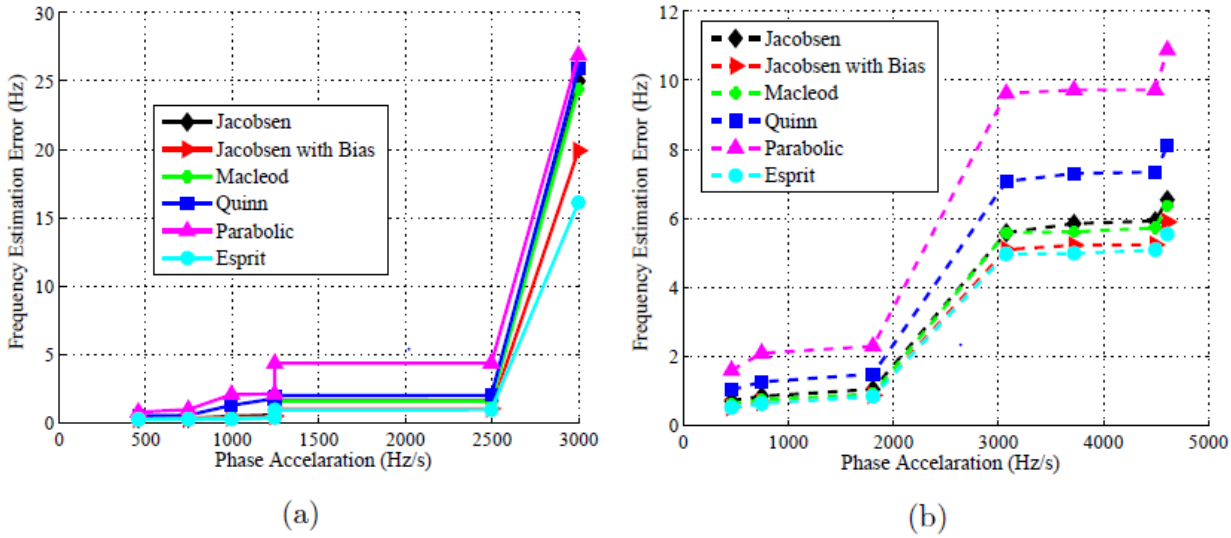

Fig 7. (a) Frequency estimation error versus phase acceleration for different estimation algorithms of the SSF sampling scheme. System parameters: SNR is -5 dB and sampling frequency rate is 100 Hz. (b) Frequency estimation error versus phase acceleration for different estimation algorithms of the MSF sampling scheme. System parameters: The SNR is -5 dB and sampling frequencies are 30 Hz and 40 Hz.

sampling schemes. It also shows that the ESPRIT and Jacobsen with Bias estimation methods lead to an improved accuracy.

However, by increasing phase acceleration value, the RMSE value is also increased. As shown in Fig. 7(a), the curve is smooth at phase acceleration below 2500 Hz/s. From 2500 Hz/s to 3000 Hz/s, due to the fast acceleration of phase, the frequency estimation methods do not follow any frequency change correctly. Therefore, the RMSE value increases sharply with the increase in phase acceleration value.

Fig. 7(b) shows RMSE versus phase acceleration for the six frequency estimation methods based on the MSF sampling scheme. We see that at high phase acceleration, the ESPRIT and Jacobsen with Bias methods clearly have smaller RMSE value than other methods.

Fig. 8 illustrates the benefit of the MSF sampling method in receiver by comparing the frequency estimation error obtained by both the SSF and MSF sampling schemes. At high phase acceleration (3000 Hz/s), the MSF scheme performs better than SSF frequency scheme. Obviously, as also observed from Fig. 8, when we try to increase the value of phase acceleration, RMSE of all frequency estimation algorithms is also increased.

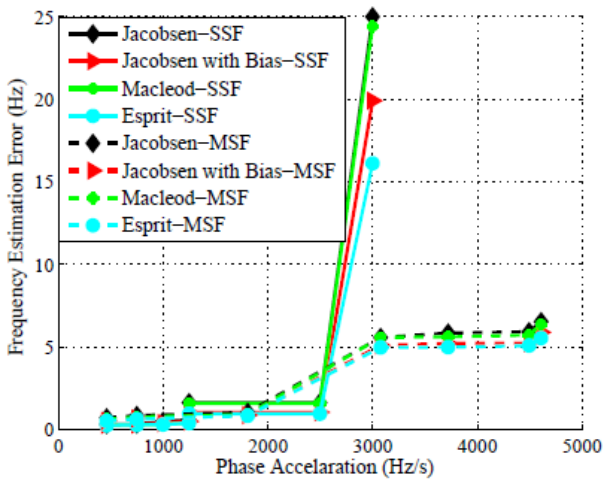

Fig 8. Comparing the frequency estimation error for different estimation algorithms of both SSF and MSF sampling schemes. System parameters: The SNR is -5 dB and sampling frequencies are 100 Hz and 30 Hz and 40 Hz for both SSF and MSF sampling schemes, respectively.

5- Computational Complexity

FFT-based algorithms to obtain accurate frequency use three samples around the peak in the FFT-based spectrum. Therefore, the computational complexity of the FFT-based algorithms have the order of $O(N \log 2(N))$ operations, where N is the number of FFT points. In the simulation, N is set to 4. Computing the ESPRIT algorithm would require the order of $O(N^3)$ operations. Therefore, for higher number of N, the ESPRIT algorithm has higher computational complexity than the FFT-based algorithms. Due to high variations of signal phase and frequency in the troposphere layer, we can set lower values for N such as 4 and 8 samples. Therefore, for the smaller value of N, the computational complexity of two algorithms are low and the computational complexity does not restrict us in choosing frequency estimation algorithm. In Table 2, the computational complexity of each frequency estimation algorithm is shown for the SSF and MSF sampling schemes.

6- Summary and Conclusions

One of the challenges in tracking RO signals of OL approach is the excess Doppler shift estimation accuracy. In order to properly estimate the frequency of a signal, sampling rate must be greater than or equal to the largest frequency component. However, in some cases, the excess Doppler

Table 2. The computational complexity of each frequency estimation algorithm for SSF (sampling rate is 100 Hz) and MSF (sampling rates are 30 Hz and 40 Hz concurrent) sampling schemes

Method	Real-time	Anti-noise capability	Computational complexity	Estimation accuracy	Number of samples (SSF)	Number of samples (MSF)
Jacobsen	Good	Moderate	$O(N\log_2(N))$	Moderate	40× 100	40× (30+40)
Jacobsen with Bias	Good	Good	$O(N\log_2(N))$	Good	40× 100	40× (30+40)
Macleod	Good	Moderate	$O(N\log_2(N))$	Moderate	40× 100	40× (30+40)
Quinn	Good	Bad	$O(N\log_2(N))$	Bad	40× 100	40× (30+40)
Parabolic	Good	Bad	$O(N\log_2(N))$	Bad	40× 100	40× (30+40)
Esprit	Bad	Good	$O(N^3)$	Good	40× 100	40× (30+40)

of RO signals is greater than the considered sampling rate which results in frequency ambiguities. For resolving these ambiguities related to the estimation of excess Doppler, in this paper, we investigated the MSF sampling method at the GNSS receivers for the first time. This method removes ambiguities by increasing the frequency estimation range and decreasing the number of samples. In other words, the sampling rate is equal to the signal bandwidth in SSF, while in this method, the bandwidth is less than that of the sampling rate. Consequently, by using MSF, we can save the radio resources like power budget and bandwidth by decreasing the required number of samples that should be transmitted from the LEO to the ground post–processing center.

Then, six different high-accuracy frequency estimation methods, Jacobsen, Jacobsen with Bias, Macleod, Quinn, Parabolic and ESPRIT, were compared for both the SSF and MSF sampling schemes from the performance and computational complexity perspective. Based on the simulation results, at low SNR, the SSF sampling scheme provides better results than that of the MSF sampling method while at moderate and high SNR, the MSF sampling scheme provides better results. We also show that, our proposed MSF method has better performance than the SSF method at the whole SNR range for a given bandwidth. Besides, using simulation results, we showed that when the phase acceleration is high, the MSF sampling scheme has better performance than that of the SSF sampling scheme. In this situation, the MSF sampling scheme should be applied since it has the lowest computational cost and better performance. On the other hand, when the level of phase acceleration is moderate or high, the MSF sampling scheme outperforms the SSF sampling scheme (with a lower computational cost).

References

[1] P.Bauer, G. Radn´oti, S. Healy, C. Cardinali, GNSS radio occultation constellation observing system experiments, Monthly Weather Review 142 (2) (2014) 555–572.

[2] A. Finger, Satellite positioning and navigation: Fundamentals, operation and application of global navigation satellite systems, AEUE-International Journal of Electronics and Communications 7 (64) (2010) 694–695.

[3] C. Ao, G. Hajj, T. Meehan, D. Dong, B. Iijima, A. Mannucci, E. Kursinski, Rising and setting GPS occultations by use of open-loop tracking, Journal of Geophysical Research: Atmospheres 114 (D4) (2009).

[4] G. Beyerle, F. Zus, Open-loop GPS signal tracking at low elevation angles from a ground-based observation site, Atmospheric Measurement Techniques 10 (1) (2017) 15-34.

[5] Wang, Kuo-Nung, et al., Open-Loop Tracking of Rising and Setting GPS Radio-Occultation Signals From an Airborne Platform: Signal Model and Error Analysis, IEEE Transactions on Geoscience and Remote Sensing 54 (7) (2016) 3967–3984.

[6] Sokolovskiy, Sergey V., Tracking tropospheric radio occultation signals from low Earth orbit, Radio Science 36 (3) (2001) 483–498.

[7] Helm, Achim, et al., GORS-A GNSS occultation, reflectometry and scatterometry space receiver, ION GNSS 2007 (2007): 2011-2021.

[8] Sokolovskiy, S. V., et al., Observing the moist troposphere with radio occultation signals from COSMIC, Geophysical Research Letters 34(18) (2007).

[9] Sokolovskiy, Sergey V., Modeling and inverting radio occultation signals in the moist troposphere., Radio Science 36 (3) (2001): 441-458.

[10] Sokolovskiy, S., et al., Post processing of L1 GPS radio occultation signals recorded in open-loop mode, Radio science 44(2) (2009): 1-13.

[11] Sokolovskiy, S., et al., GPS profiling of the lower troposphere from space: Inversion and demodulation of the open-loop radio occultation signals, Geophysical Research Letters 33(14) (2006).

[12] Wang, Kuo-Nung., Signal analysis and radio holographic methods for airborne radio occultations, Ph.D. thesis, Purdue University (2015).

[13] Gorbunov, M. E., Radio-holographic analysis of Microlab-1 radio occultation data in the lower troposphere, Journal of Geophysical Research: Atmospheres 107.D12 (2002): ACK-7.

[14] Kursinski, E. Robert, et al., The GPS radio occulation technique, TAO 11 (1) (2000) 53–114.

[15] M. Gorbunov, Canonical transform method for processing radio occultation data in the lower troposphere, Radio Science 37 (5) (2002): 9-1

[16] M. E. Gorbunov, L. Kornblueh, Analysis and validation of GPS/MET radio occultation data, Journal of Geophysical Research: Atmospheres 106 (D15) (2001) 17161–17169.

[17] Jensen, Arne Skov, et al., Full spectrum inversion of radio occultation signals, Radio Science 38 (3) (2003) 6–1.

[18] Adhikari, Loknath, Feiqin Xie, and Jennifer S. Haase, Application of the full spectrum inversion algorithm to simulated airborne GPS radio occultation signals, Atmospheric Measurement Techniques 9 (10) (2016) 5077-5087.

[19] Gorbunov, M. E., K.B. Lauritsen, Analysis of wave fields by Fourier integral operators and their application for radio occultations, Radio Science 39 (4) (2004): 1-15.

[20] Jensen, Arne Skov, et al, Geometrical optics phase matching of radio occultation signals, Radio science 39 (3) (2004).

[21] Hocke, K., et al., Radio occultation data analysis by the radio holographic method, Journal of Atmospheric and Solar-Terrestrial Physics 61 (15) (1999) 1169–1177.

[22] Sokolovskiy, S., et al., On the uncertainty of radio occultation inversions in the lower troposphere, Journal of Geophysical Research: Atmospheres 115 (D22) (2010).

[23] Sørensen, Mikael, and Lieven De Lathauwer., Multidimensional harmonic retrieval via coupled canonical polyadic decomposition—Part II: Algorithm and multirate sampling, IEEE Transactions on Signal Processing 65(2) (2016): 528-539.

[24] Stoica, Petre, and Randolph L. Moses, Introduction to spectral analysis, Pearson Education, (1997).
[25] Marple Jr, S. Lawrence, and William M. Carey, Digital spectral analysis with applications, (1989): 2043-2043.
[26] Cui, Kaibo, et al., DOA estimation of LFM signals based on STFT and multiple invariance ESPRIT, AEU-International Journal of Electronics and Communications 77 (2017) 10–17.
[27] Y. Tian, X. Sun, Passive localization of mixed sources jointly using MUSIC and sparse signal reconstruction, AEU-International Journal of Electronics and Communications 68 (6) (2014) 534–539.
[28] B. G. Quinn, Estimating frequency by interpolation using Fourier coefficients, IEEE Transactions on Signal Processing 42 (5) (1994) 1264–1268.
[29] M. D. Macleod, Fast nearly ML estimation of the parameters of real or complex single tones or resolved multiple tones, IEEE Transactions on Signal processing 46 (1) (1998) 141–148.
[30] Y. Zakharov, V. Baronkin, T. Tozer, DFT-based frequency estimators with narrow acquisition range, IEE Proceedings-Communications 148 (1) (2001) 1–7.
[31] E. Aboutanios, S. Reisenfeld, Frequency estimation and tracking for low earth orbit satellites, in: IEEE VTS 53rd Vehicular Technology Conference, Proceedings (Cat. No. 01CH37202). Vol. 4. IEEE, (2001).
[32] B. G. Quinn, Estimation of frequency, amplitude, and phase from the DFT of a time series, IEEE transactions on Signal Processing 45 (3) (1997) 814–817.
[33] L. Mohammadi, S. Amiri, Performance Analysis of Different Frequency Estimation Methods in GNSSRO Receivers with Open Loop Tracking, The Modares Journal of Electrical Engineering 13 (2) (2013) 26–39.
[34] Jacobsen, Eric, and Peter Kootsookos., Fast, accurate frequency estimators [DSP Tips & Tricks]. IEEE Signal Processing Magazine 24(3) (2007): 123-125.
[35] Teukolsky, Saul A., et al., Numerical recipes in C., SMR 693.1 (1992): 59-70.
[36] Voglewede, Paul, Parabola approximation for peak determination, Global DSP Magazine 3(5) (2004): 13-17.
[37] Candan, Çagatay, A method for fine resolution frequency estimation from three DFT samples, IEEE Signal processing letters 18.6 (2011): 351-354.
[38] Roy, Richard, and Thomas Kailath, ESPRIT- estimation of signal parameters via rotational invariance techniques, IEEE Transactions on acoustics, speech, and signal processing 37(7) (1989): 984-995.
[39] Roy, Robert, Arogyaswami Paulraj, and Thomas Kailath, ESPRIT-A subspace rotation approach to estimation of parameters of cissoids in noise, IEEE transactions on acoustics, speech, and signal processing 34(5) (1986): 1340-1342.
[40] M. E. Gorbunov, A. S. Gurvich, L. Kornblueh, Comparative analysis of radio holographic methods of processing radio occultation data, Radio science 35 (4) (2000) 1025–1034.
[41] Priebe, Les, Mark Philip Swenholt, and Ronald Persson, Use of multiple sample frequencies to resolve ambiguities in band-folded digital receivers, U.S. Patent No. 6,031,869. 29 Feb. 2000.
[42] H. Lee, H.-G. Ryu, Compensation of RF impairment in multi-band receiver based on RF sub-sampling, AEU-International Journal of Electronics and Communications 66 (8) (2012) 613–618.
[43] M. R. Yuce, A. Tekin, W. Liu, Design and performance of a wideband sub-sampling front-end for multi-standard radios, AEU-International Journal of Electronics and Communications 62 (1) (2008) 41–48.

HOW TO CITE THIS ARTICLE

L. Mohammadi, SH. Amiri, A Novel Sampling Approach in GNSS-RO Receivers with Open Loop Tracking Method, AUT J. Elec. Eng., 51(2) (2019) 161-170.

DOI: 10.22060/eej.2019.15766.5267